ISSN 0036-0295, Russian Metallurgy (Metally), Vol. 2020, No. 5, pp. 573–578. © Pleiades Publishing, Ltd., 2020.
Russian Text © The Author(s), 2020, published in Metally, 2020, No. 3, pp. 77–83.

Formation of a Gradient Structure in a Material by Twist Extrusion

O. V. Prokof'eva[a], *, Y. Y. Beygelzimer[b], **, V. V. Usov[c], *, N. M. Shkatulyak[c], T. S. Sovkova[c], A. N. Sapronov[a], D. V. Prilepo[a], and V. N. Varyukhin[a]**

[a] *Donetsk Institute for Physics and Engineering named after A.A. Galkin, Donetsk, Ukraine*

[b] *Donetsk Institute for Physics and Engineering named after A.A. Galkin, National Academy of Sciences of Ukraine, Kyiv, Ukraine*

[c] *Ushinskii South-Ukrainian National Pedagogical University, Odessa, Ukraine*

**e-mail: prokofok@mail.ru*

***e-mail: yanbeygel@gmail.com*

****e-mail: valentinusov67@gmail.com*

Received August 2, 2018; revised November 27, 2018; accepted December 17, 2018

Abstract—Hexagonal samples with an initial coarse-grained structure (CG) in the near-axis zone and a gradient ultrafine-grained (UFG) structure at the periphery are formed by twist extrusion (TE) of commercial-purity copper through a hexagonal twist die with a small twist-line slope. This hybrid structure of the samples provides conditions for a large uniform deformation before necking (due to the CG core) and a high yield strength (due to the gradient UFG periphery). The hybrid CG–UFG structure can be formed due to the threshold nature of metal grain refinement during cyclic deformation. A simple relation is derived for estimating the CG core diameter of the sample. The structure and the texture of the samples are investigated by X-ray diffraction and optical microscopy.

Keywords: gradient material, coarse-grained structure, ultrafine grained structure, twist extrusion, crystallographic texture, substructural characteristics, inverse pole figures

DOI: 10.1134/S0036029520050110

INTRODUCTION

Materials with a gradient structure include the materials in which the size of structural elements gradually increases from a ultrafine grained (UFG) level near the surface to a coarse-grained (CG) level in the inner layers [1, 2]. These materials are technically attractive because of their high mechanical properties [3–10]. Therefore, the processes that are involved in the formation of a gradient structure in metals and alloys are of interest.

Gradient structures can be formed, in particular, by severe plastic deformation [11, 12], achieving a gradient in a strain distribution. For example, plates and rods with an UFG layer are produced by surface mechanical attrition [13, 14] and plastic flow machining [15]. Gradient structures in cylindrical copper and magnesium rods were formed by three-roll planetary milling at large strains (also known as radial-shift rolling) [16, 17].

Mathematical simulation [18] showed possible formation of metal rods with an UFG shell and a CG core by twist extrusion (TE) [19]. The advantage of the method is the possibility to manage the outer UFG layer thickness even up to the transition of the entire cross section of the sample to an UFG state. This is important in the case when rods are machined after their deformation to remove part of the surface layer, for example, for threading.

The aim of this work is to study the possibilities of TE to form gradient materials by the example of a copper bar with a hexagonal cross section.

SUBSTANTIATION OF THE TECHNIQUE

The idea to use TE to produce rods with an UFG shell and a CG core relies on the threshold nature of metal grain refinement during cyclic deformation [20–23]. This effect stems from the fact that deformation reversal discharges dislocation pileups, which lead to the formation of high-angle boundaries. Grain refinement during reverse deformation begins only after the formation of a sufficient number of new dislocation pileups. Therefore, reversal decreases the efficiency of deformation-induced grain refinement. If the strain amplitude is too low for the required volume of dislocation pileups to form in a loading half cycle, no high-

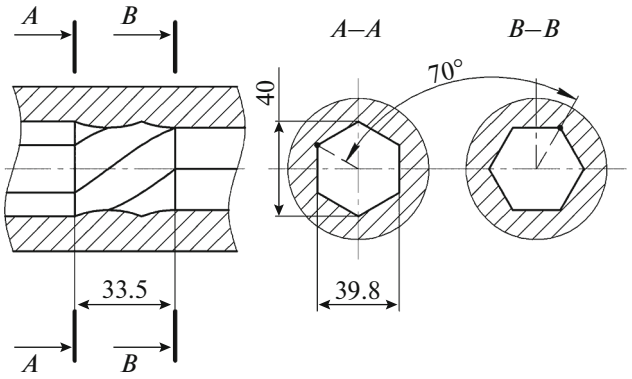

Fig. 1. Schematic of the twist die channel used for the production of a gradient material.

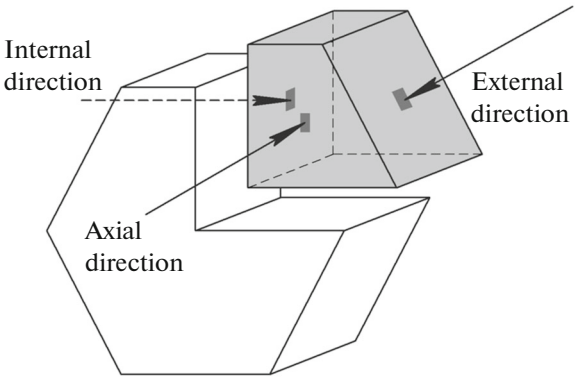

Fig. 2. Schematic diagram of cutting a template. The arrows indicate the direction of XRD investigation. The rectangles on the corresponding sides of the sample indicate the location of the irradiated area.

angle boundaries form. Thus, grain refinement has an amplitude threshold during cyclic deformation [18].

The finite element method calculations showed that TE-induced deformation (simple shear along the plane that is perpendicular to the extrusion axis) took place at the borders of the twist section of the twist die [19, 24]. The sign of the shear strain for a fixed material point when it leaves the twist section is opposite to that when the point enters into the twist section; i.e. the deformation during TE is cyclic. Shear strain amplitude γ at distance r from the extrusion axis is determined by the ratio

$$\gamma = (r/R)\tan\beta, \quad (1)$$

where R is the distance from the axis to the most distant point of the cross section and β is the angle between the trajectory of this point and the axis.

The further the material point from the axis, the more valid the described model and correlation (1) [25].

Assume that γ^* is the mentioned threshold of the shear strain amplitude below which grain refinement does not occur. Let us denote

$$r^* = R\gamma^*/\tan\beta. \quad (2)$$

Then, Eqs. (1) and (2) suggest that an UFG structure forms in the material at a distance $r > r^*$ from the extrusion axis after a sufficiently large number of TE passes, and the microstructure is still in a CG state at $r < r^*$.

Simple Eq. (2) allows us to estimate the position of the interface between UFG and CG zones when it is relatively far away from the extrusion axis. The inaccuracy of this ratio increases when the interface between microstructures approaches the axis, because the TE model becomes incorrect.

EXPERIMENTAL

Prismatic commercial-purity copper (M1) billets with a hexagonal cross section 40 mm in diameter and 80 mm in length were extruded. The initial material was prepared by hot rolling and annealed at 550°C for 1 h. TE was carried out at room temperature using a hexagonal twist die with a twist-line slope of 40° (Fig. 1). The treatment included one or four TE passes through a die at an applied backpressure of ~100 MPa.

Six-sided templates 10 mm thick were cut from the middle of the extruded samples perpendicular to the TE axis. The templates were examined by optical microscopy and X-ray diffraction (XRD). The Vickers hardness of the templates was measured using a HV-5 hardness tester at a load of 49 N (5 kgf) for 30 s. The hardness distribution was determined along the cross-sectional diameter.

The etched ($HCl + FeCl_3 + H_2O$ reagent) surface of the templates was examined using a Carl Zeiss Axiovert 40 MAT optical microscope to estimate the length of an UFG layer. A 5-mm-long panoramic image of the structure was composed by joining sequentially taken photos.

The fourth part of the template was used for XRD studies. The texture and the substructure characteristics (coherent domain size (CDS), lattice microdistortion $\varepsilon = \Delta a/a$) in three directions indicated in Fig. 2 were analyzed. We examined the texture by XRD in the Bragg–Brentano geometry and constructed inverse pole figures (IPFs) [26, 27].

The initial sample, the extruded sample, and the corresponding sample without texture (reference) were analyzed by XRD using a DRON-3m diffractometer and Cu $K\alpha$ radiation in the range θ–2θ. The following XRD lines were detected: (111), (200), (220), (311), (222), (400), (331), and (420). The standard was prepared from small recrystallized copper filings after annealing in a vacuum at 400°C for 1 h. The ratios of the XRD integral intensities of the investigated samples and the standard sample, which was normalized according to Morris, were used as the pole densities in IPFs [28].

Fig. 3. Microstructure in the billet cross section after four TE passes: (a) 5-mm-long panoramic image taken along the diameter of the hexagon in the direction from the edge to the center of the cross section (from left to right) and (b) center of the cross section.

The lattice microdistortions and CDSs were determined by the approximation method [26]. According to the method, the intrinsic broadening of the same diffraction lines but different reflection orders are compared to determine the microstrain anisotropy and CDSs along different crystallographic directions that coincide with the directions under study.

RESULTS AND DISCUSSION

Figure 3a shows a panoramic image of the microstructure from the edge to the center of the cross section. At the given scale, the transition from a fine-grained structure in the surface region (on the left) to a coarse-grained structure at a distance of 5 mm from the edge of the cross section (on the right) is clearly visible. Figure 3b shows the central area of the cross section at the same scale for comparison. We can say that the microstructure at a distance of about 5 mm from the billet surface after four TE passes is almost of the same quality as that at the center of the cross section.

The Vickers hardness distribution along the sample diameter (Fig. 4) has an almost horizontal region at $r < 10$ mm, which is adjacent to the axis. In the range 10 mm $< r <$ 20 mm, the hardness increases rapidly towards the sample surface. The $HV(r)$ dependence does not change with increasing number of TE passes from one to four.

The results obtained are in agreement with the concepts described above. If we assume that $r^* = 10$ mm, the shear strain amplitude calculated by Eq. (2) is $\gamma^* = 0.42$. This estimate agrees well with the strain threshold, which was selected in [18] after analysis of literature sources.

Table 1 lists the parameters of the substructure after four TE passes. Plastic deformation is known to cause XRD lines to widen compared to those of an undeformed or annealed metal. This widening is caused by CDS refinement (size <1 μm) and lattice microdistortions. Table 1 suggests that there is anisotropy of both the CDS and the lattice microdistortion (therefore, the microstress).

CDSs in the axial direction (see Fig. 2) in the crystallographic ⟨111⟩ directions, which coincide with the pressing axis, were 0.99 μm, and these sizes in the ⟨200⟩ directions, which coincide with the extrusion axis, were 0.11 μm. More severe grain refinement in the ⟨200⟩ directions, the volume fraction of which is large in the extrusion axis direction (Fig. 5a), provided a lower level of lattice microdistortions in the ⟨200⟩ directions (7.69×10^{-4}) in comparison with the ⟨111⟩ direction (9.95×10^{-4}).

The CDSs in the ⟨111⟩ directions, which coincide with the internal radial direction of measurement (see

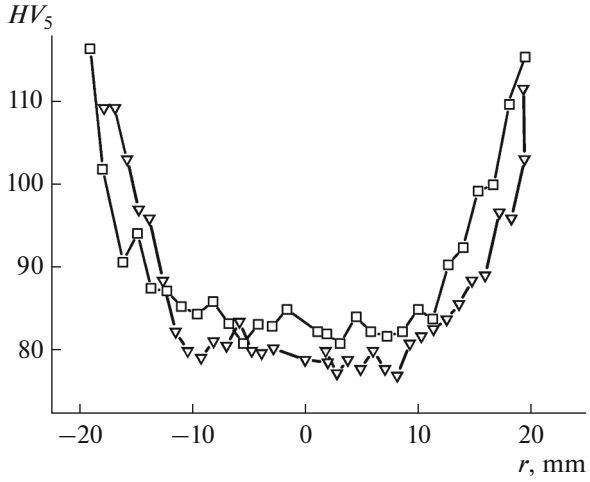

Fig. 4. Vickers hardness as a function of the coordinate along the diameter of the hexagonal cross section of the billet: (▽) one TE pass and (□) four TE passes.

Table 1. CDS D and lattice microdistortion $\Delta a/a$ measured along three directions

HKL	*D*, μm	$\varepsilon = 10^{-4}\Delta a/a$	*E*, GPa	$\sigma = E\varepsilon$, MPa
Axial measurement direction				
⟨111⟩, ⟨222⟩	0.99	9.95	123	122.4
⟨200⟩, ⟨400⟩	0.11	7.69	123	94.6
External measurement direction				
⟨111⟩, ⟨222⟩	0.92	5.61	123	69.0
⟨200⟩, ⟨400⟩	0.16	6.53	123	80.3
Internal measurement direction				
⟨111⟩, ⟨222⟩	4.1	4.56	123	56.1
⟨200⟩	0.24	3.89	123	47.8

Fig. 2), were 4.1 μm, and those in the ⟨200⟩ directions, 0.24 μm. In the external measurement direction, CDSs are even smaller, 0.92 and 0.16 μm for crystallographic directions ⟨111⟩ and ⟨200⟩, respectively. This is due to the plastic twisting deformation mechanism and the vortex movement of refined grains in the ⟨200⟩ directions to a greater extent than in the ⟨111⟩ directions.

Grain refinement is known to cause mutual grain misorientation, which manifests itself in an increase in lattice microdistortions. The microdistortions in the ⟨200⟩ direction (radial external direction) are greater than in the ⟨111⟩ direction (see Table 1). This is explained by the fact that grains are more intensively refined in the ⟨200⟩ direction, in contrast to the ⟨111⟩ direction. The situation is opposite along the internal

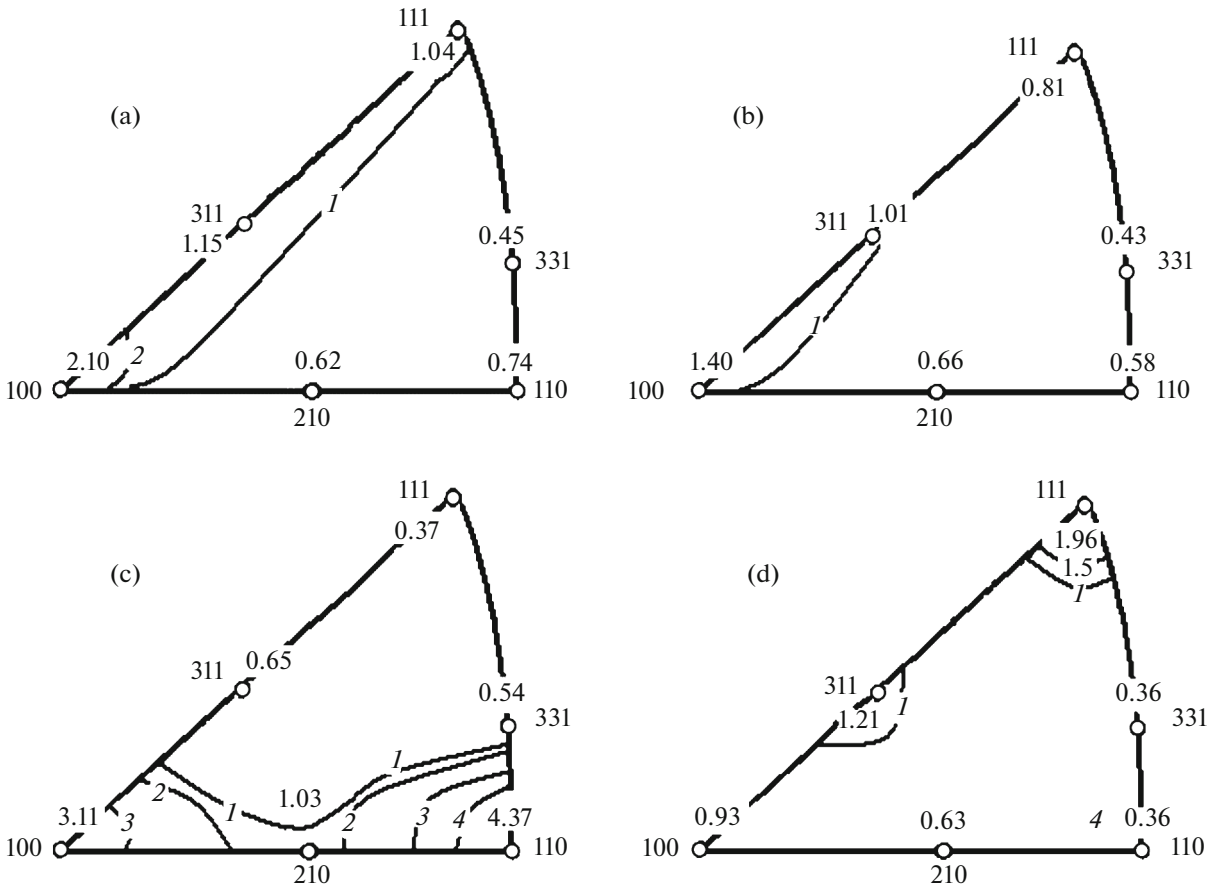

Fig. 5. Inverse pole figures after four TE passes ((a) axial direction, (b) external direction, (c) internal direction) and before TE ((d) direction perpendicular to the TE axis).

radial direction after extrusion: microdistortions in the ⟨111⟩ direction exceed those in the ⟨200⟩ directions. However, microstresses are higher in the external part than those inside the sample in both ⟨111⟩ and ⟨200⟩ directions.

The corresponding IPFs are shown in Fig. 5. Analysis of IPFs showed that mainly crystallographic directions ⟨100⟩ with scattering up to ⟨111⟩ are located parallel to the extrusion axis (Fig. 5a). Crystallographic directions ⟨100⟩ with scattering up to ⟨311⟩ are located in the external direction (Fig. 5b). The internal direction (see Fig. 5c) coincides with the crystallographic directions located along the base of the stereographic triangle ⟨100⟩–⟨110⟩ with maxima at the indicated poles. It should be noted that the angle between the planes of the internal and external regions is 30°.

The twist extrusion can be represented as a model of compression deformation along the extrusion axis and twist deformation (shear) on a plane perpendicular to the extrusion axis. As was shown in [29], the main components of the twist texture in fcc metals (for example, copper, aluminum) are {111} ⟨*uvw*⟩ (axial), {*hkl*} ⟨110⟩ (axial), and {001} ⟨110⟩. Here, the curly brackets indicate the planes in which a shear displacement occurs in twisting around the pressing axis. The angle brackets show the shear directions lying on the shear plane.

Taking this into account, let us assume that this arrangement of the pole density peaks in the IPFs of the extruded copper sample (Figs. 5a–5c) is due to the formation of twist texture components {100}⟨110⟩. Extrusion makes the texture weaker on the periphery of the sample due to the vortex movement of the fragments of refined grains. This is supported by the decrease in the pole density in the IPFs of the external side of the extruded sample (Fig. 5b). The fact that the texture of the initial cylindrical sample (Fig. 5d) differs from the above-described texture of the extruded sample is noteworthy. The crystallographic ⟨111⟩ and ⟨311⟩ directions can be seen to coincide with the cylinder axis, which have probably resulted from recrystallization of the initial sample during annealing at 500°C.

A comparison of the data (Table 1) with the results obtained at the IBR-2 pulsed reactor at the Joint Institute for Nuclear Research (Dubna) [30] showed that the level of lattice microdistortions and the regularities of their change along the radial direction of the hexagon are quite close.

CONCLUSIONS

(1) The CG structure in the near axis zone and the gradient structure in the thin layer at the periphery, where the grain size varies from an initial to a submicrocrystalline one, were formed by TE in commercial-purity copper. This possibility is caused by the fact that the shear strain amplitude in a near-axis zone of a sample at a small twist-line slope of the die does not exceed γ^*, which is the minimum necessary value for grain refinement. The ratio $r^* = R\gamma^*/\tan\beta$ gives a rough estimation of the radius of the CG zone. As closer the r^* to R (distance from the axis to the most distant point in the billet cross section), then more reliable this ratio.

(2) XRD analysis was used to determine the substructural characteristics (CDS, lattice microdistortions, lattice microstresses). The texture was analyzed. These substructural characteristics are anisotropic over the cross section of the billet. Torsional texture components {100}⟨110⟩ appeared after TE. Extrusion makes the texture weaker, the CDSs smaller, and microdistortion larger at the periphery of the sample due to the vortex movement of the fragments of the grains to be refined.

REFERENCES

1. S. Suresh, "Graded materials for resistance to contact deformation and damage," Science **292** (5526), 2447–2451 (2001).
2. D. A. Hughes and N. Hansen, "Graded nano-structures produced by sliding and exhibiting universal behavior," Phys. Rev. Lett. **87** (13), 135503–135511 (2001).
3. T. H. Fang, W. L. Li, N. R. Tao, et al., "Revealing extraordinary intrinsic tensile plasticity in gradient nanograined copper," Science **331** (6024), 1587–1590 (2011).
4. K. Lu, "Making strong nanomaterials ductile with gradients," Science **345** (6203), 1455–1456 (2014).
5. Y. J. Wei, Y. Q. Li, L. C. Zhu, et al., "Evading the strength ductility trade-off dilemma in steel through gradient hierarchical nanotwins," Nat. Commun. **5** (3580) (2014).
6. X. L. Wu, P. Jiang, L. Chen, et al., "Synergetic strengthening by gradient structure," Mater. Res. Lett. **2** (4), 185–191 (2014).
7. X. L. Wu, P. Jiang, L. Chen, et al., "Extraordinary strain hardening by gradient structure," Proc. Natl. Acad. Sci. USA. **111** (20), 7197–7201 (2014).
8. M. X. Yang, Y. Pan, F. P. Yuan, et al., "Back stress strengthening and strain hardening in gradient structure," Mater. Res. Lett. **4** (3), 141–151 (2016).
9. X. Bian, F. Yuan, Y. Zhu, and X. Wu, "Gradient structure produces superior dynamic shear properties," Mater. Res. Lett. **5** (7), 501–507 (2017).
10. J. J. Li, G. J. Weng, S. H. Chen, and X. L. Wu, "On strain hardening mechanism in gradient nanostructures," Intern. J. Plasticity. **88**, 89–107 (2017).
11. R. Z. Valiev, Y. Estrin, Z. Horita, T. G. Langdon, M. J. Zehetbauer, and Y. T. Zhu, "Producing bulk ultrafine-grained materials by severe plastic deformation: ten years later," JOM **68**, 1216–1226 (2016).
12. Y. Estrin and A. Vinogradov, "Extreme grain refinement by severe plastic deformation: a wealth of challenging science," Acta Mater. **61**, 782–817 (2013).
13. K. Lu and J. Lu, "Nanostructured surface layer on metallic materials induced by surface mechanical attrition

treatment," Mater. Sci. Eng. A. **375–377**, 38–45 (2004).

14. Z. Yin, X. Yang, X. Ma, et al., "Strength and ductility of gradient structured copper obtained by surface mechanical attrition treatment," Mater. Design. **105**, 89–95 (2016).
15. V. Q. Vu, Y. Beygelzimer, L. S. Toth, J.-J. Fundenberger, R. Kulagin, and C. Chen, "The plastic flow machining: a new SPD process for producing metal sheets with gradient structures," Mater. Characterization **138**, 208–214 (2018).
16. Y. L. Wang, A. Molotnikov, M. Diez, R. Lapovok, H. E. Kim, J. T. Wang, and Y. Estrin, "Gradient structure produced by three roll planetary milling: numerical simulation and microstructural observations," Mater. Sci. Eng. A. **639**, 165–172 (2015).
17. M. Diez, H. J. Kim, V. N. Serebryanyi, S. V. Dobatkin, and Y. Estrin, "Improving the mechanical properties of pure magnesium by three-roll planetary milling," Mater. Sci. Eng. A **612**, 287–292 (2014).
18. O. V. Prokof'eva, Y. Y. Beygelzimer, R. Y. Kulagin, Y. Z. Estrin, and V. N. Varyukhin, "Producing of ultrafine grained composites with a large uniform elongation by twist extrusion: mathematical simulation," Russ. Metall. (Metally), No. 3, 226–230 (2017).
19. Y. Beygelzimer, R. Kulagin, Y. Estrin, et al., "Twist extrusion as a potent tool for obtaining advanced engineering materials: a review," Adv. Eng. Mater. (2017). https://doi.org/10.1002/adem.201600873
20. D. Orlov, Y. Todaka, M. Umemoto, Y. Beygelzimer, Z. Horita, and N. Tsuji, "Plastic flow and grain refinement under simple shear-based severe plastic deformation," Mater. Sci. Forum **604–605**, 171–178 (2009).
21. D. Orlov, Y. Todaka, M. Umemoto, and N. Tsuji, "Role of strain reversal in grain refinement by severe plastic deformation," Mater. Sci. Eng. A. **499**, 427–433 (2009).
22. H. Petryk and S. Stupkiewicz, "A quantitative model of grain refinement and strain hardening during severe plastic deformation," Mater. Sci. Eng. A **444**, 214–219 (2007).
23. Y. Beygelzimer, "Grain refinement versus voids accumulation during severe plastic deformation of polycrystals: mathematical simulation," Mech. Mater. **37**, 753–767 (2005).
24. Y. Beygelzimer, V. Varyukhin, R. Kulagin, and D. Orlov, "Twist extrusion: review," Fiz. Tekh. Vys. Davlenii. **25** (3–4), 8–37 (2015).
25. M. I. Latypov, M.-G. Lee, Y. Beygelzimer, R. Kulagin, and H. S. Kim, "Simple shear model of twist extrusion and its deviations," Met. Mater. Intern. **21** (3), 569–579 (2015).
26. *Diffraction Analysis of the Microstructure of Materials*, Ed. by E. J. Mittemeijer and P. Scardi (Springer, 2004).
27. R. Guinebretiere, *X-ray Diffraction by Polycrystalline Materials* (Wiley, 2013).
28. Ya. D. Vishnyakov, A. A. Babareko, S. A. Vladimirov, and I. V. Egiz, *Texture Formation Theory in Metals and Alloys* (Nauka, Moscow, 1979).
29. G. R. Canova, "Theory of torsion texture development," Acta Metall. **32** (2), 211–226 (1984).
30. O. V. Prokof'eva, D. V. Prilepo, G. D. Bokuchava, A. Kh. Islamov, A. N. Sapronov, and A. S. Doroshkevich, "Formation of a submicro and coarse-grained structure in metals by twist extrusion," Fiz. Tekh. Vys. Davlenii. **28** (1), 13–22 (2018).

Translated by T. Gapontseva